

Phase Match for Out-of-Distribution Generalization

Chengming Hu Rui Wang Hao Chen Zhouwang Yang*

University of Science and Technology of China

{cmhu, rui_wang, ch330822}@mail.ustc.edu.cn, yangzw@ustc.edu.cn

Abstract

The Fourier transform, serving as an explicit decomposition method for visual signals, has been employed to explain the out-of-distribution generalization behaviors of Convolutional Neural Networks (CNNs). Previous research and empirical studies have indicated that the amplitude spectrum plays a decisive role in CNN recognition, but it is susceptible to disturbance caused by distribution shifts. On the other hand, the phase spectrum preserves highly-structured spatial information, which is crucial for visual representation learning. In this paper, we aim to clarify the relationships between Domain Generalization (DG) and the frequency components by introducing a Fourier-based structural causal model. Specifically, we interpret the phase spectrum as semi-causal factors and the amplitude spectrum as non-causal factors. Building upon these observations, we propose Phase Match (PhaMa) to address DG problems. Our method introduces perturbations on the amplitude spectrum and establishes spatial relationships to match the phase components. Through experiments on multiple benchmarks, we demonstrate that our proposed method achieves state-of-the-art performance in domain generalization and out-of-distribution robustness tasks.

1. Introduction

Convolutional Neural Networks (CNNs) have demonstrated exceptional performance on various visual downstream tasks, assuming the typical independent and identically distributed (i.i.d.) setting for training and testing data [9, 22]. However, in real-world scenarios, the CNNs often exhibit subpar performance due to random and uncertain distribution shifts, also known as domain shifts, between the training and testing data. Consequently, researchers have introduced Domain Generalization (DG) [31], an approach that aims to enable machine learning models to generalize to unseen data distributions, attracting increasing attention in recent times.

*Corresponding author

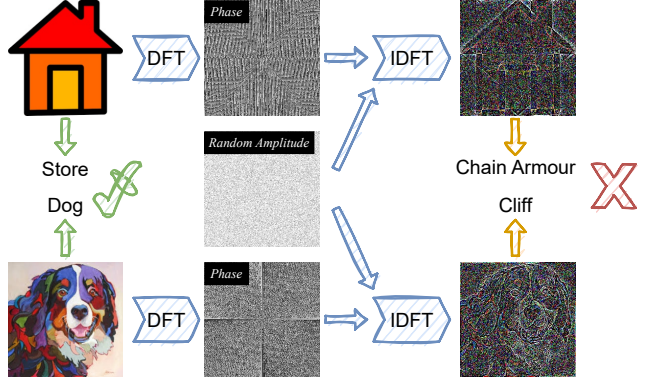


Figure 1. In this toy-example experiment, we generate corrupted images from the phase spectra of the raw images and a randomly initialized amplitude spectrum. For ResNet-18 without effective training, the raw images are (semi)correctly predicted to *store* and *dog*, while the CNN classifies the corrupted images as *chain armour* and *cliff* respectively.

Mainstream Domain Generalization (DG) studies [1, 20, 25, 29, 30, 30, 38] primarily focus on extracting invariant representations from source domains that can be effectively generalized to the target domain, which remains inaccessible during training. Another approach involves data augmentation [17, 19, 27, 33, 54, 57, 61], a technique to simulate domain shifts or attacks without altering the label. Data augmentation can also be viewed as a means to compel the network to extract invariant representations under various perturbations (*e.g.*, flip, brightness, contrast, style).

Recent studies [3, 10, 28, 42, 47] have focused on exploring the explanations for CNN’s generalizability in the frequency domain. These experiments have demonstrated the sensitivity of CNNs to the amplitude spectrum. In Fig. 1, we present our toy-example experiment, initializing a random amplitude spectrum, and reconstructing the images using their phase spectrum. Our observations reveal that the ResNet-18 [15] pre-trained on ImageNet-1K [5] (semi)correctly predicts the categories of raw images (indicated by green arrows), but inaccurately predicts the category of the reconstructed images (indicated by yellow ar-

rows). In contrast, the human visual system remains proficient in recognizing objects (*e.g.*, house and dog) in the reconstructed image despite extreme corruptions, suggesting that the amplitude spectrum does not significantly impact recognition and localization. Based on these observations, we draw two conclusions: (1) existing pre-trained CNNs heavily rely on the amplitude spectrum, and (2) the amplitude information is redundant as a visual signal for the human visual system. Consequently, eliminating the influence of amplitude information can substantially improve the signal-to-noise ratio (SNR) and enhance the network’s representation learning capabilities.

Additionally, it is essential to note that the reconstructed images still preserve highly structured spatial information. For each *patch* in the image pairs, the structural information (*e.g.*, contour, edge) remains remarkably consistent, which significantly contributes to recognition and positioning tasks. However, existing studies have largely overlooked the spatial information preserved in the image patches. Taking into account the invariance of phase spectra and humans’ successful prediction outcomes, we assert that the secret to robust visual systems lies in the utilization of the phase spectrum, which effectively preserves spatial information in an image. Consequently, establishing spatial relationships for the phase spectrum becomes a critical aspect of achieving a generalizable and robust network.

This paper addresses Domain Generalization (DG) problems from the frequency perspective and introduces *Phase Match* (PhaMa) as shown in Fig. 3. To enhance generalizability against amplitude perturbations caused by domain shifts, we adopt perturbations on the amplitude spectrum for adversarial training. Specifically, we randomly select two images from the source domains and mix their amplitude spectra using linear interpolation. Both the original images and the augmented versions are then fed into the network. Subsequently, we introduce a patch contrastive loss [37] to encourage matching of patch representations from the image pairs. This approach further alleviates the impact of the amplitude component and establishes the spatial relationship of the phase spectrum, allowing the network to prioritize the phase spectrum of the image.

Our contributions are summarized as: (1) We present an intuitive causal view for domain generalization with the Fourier transform and specify the causal/non-causal factors with association to the Fourier spectrum, (2) a method called *Phase Match* is proposed to enforce the network to focus more on the phase spectrum for generalizable representation learning, and (3) results from comprehensive experiments show that our method outperforms state-of-the-art methods on many DG benchmarks.

2. Related Work

Domain Generalization. Domain generalization (DG) aims to learn a model from the source domains that has high performance in unseen target domains. Data augmentation is a widely used technique in machine learning to enhance the out-of-distribution generalization ability of the models [48, 59]. MixUP [57] adopts linear interpolations between two input samples and smooth the label. CutMix [54] generates training images by cutting and pasting from raw images. From the frequency perspective, recent works [3, 29, 51] utilize the property of phase and amplitude of the Fourier spectrum into DG [29, 51] and Robustness [3]. Motivated by the observation that image style can be captured from latent feature statistics [19, 44], many DG methods utilize adaptive instance normalization (AdaIN) [19] and its variants [27, 33, 61] to synthesize novel feature statistics. Another way to tackle DG problems is domain-invariant representation learning. For example, MMD-AAE [25] regularizes a multi-domain autoencoder by minimizing the Maximum Mean Discrepancy (MMD) distance. [58] minimizes the KL divergence between the conditional distributions of different training domains. DAL [38] disentangles domain-specific features using adversarial losses. Recently, contrastive learning is introduced into DG. PDEN [26] utilizes contrastive learning for single domain generalization. SelfReg [21] aligns the positive pairs by contrastive learning. PCL [53] proposes a proxy-based contrastive learning method for DG.

CNN Behaviours from Frequency Perspective. A wide range of frequency-based researches on CNN have been conducted. [10] conducts adversarial attacks on low-frequency components and reveals that CNN only utilize the low-frequency components for prediction. [42] demonstrates that CNN is vulnerable under low-frequency perturbations. On the other hand, [47] observes that high-frequency components is important to the generalization of CNN. Further, APR [3] offers a qualitative study for both amplitude and phase spectrum, and argues that the phase spectrum is crucial for robust recognition. However, the spatial relationships of the phase spectrum remains unclear, which we aim to explore from a contrastive view.

Contrastive Learning. As a simple and powerful tool for visual representation learning, there has been a surge of impressive studies [2, 4, 14, 49] on contrastive learning [11]. The only prerequisite of contrastive learning is a definition of positive-negative pairs. InstDisc [49] uses a memory-bank to store the features for contrast. MoCo [14] builds a dictionary with a queue and a momentum update encoder. SimCLR [4] introduces a learnable projection head between encoder networks and the contrastive loss. DINO [2] trains the Vision Transformer (ViT) [6], which contains explicit information about the semantic segmentation.

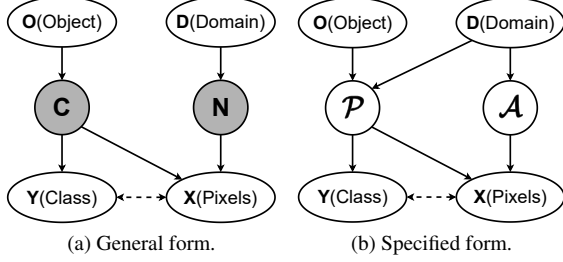


Figure 2. Structural causal models for DG. Solid arrow denotes the parent node causes the child node; dash arrow denotes correlation; shaded variables are unobserved.

3. Method

3.1. Problem Definition

Given a training set consisting of M source domains $\mathcal{D}_s = \{\mathcal{D}_i | i = 1, \dots, M\}$ where $\mathcal{D}_i = \{(x_i^j, y_i^j)\}_{j=1}^{n_i}$ denotes the i -th domain. The goal of domain generalization is to learn a robust and generalizable model $g : \mathcal{X} \rightarrow \mathcal{Y}$ from the M source domains and achieve a minimum prediction error on the target domain \mathcal{S}_t , which is inaccessible during training:

$$\min_g \mathbb{E}_{(x,y) \in \mathcal{D}_t} [\ell(g(x), y)]. \quad (1)$$

In this paper, we consider an object recognition model $g(\cdot; \theta) : \mathcal{X} \rightarrow \mathbb{R}^N$ comprising an encoder E and a classifier C , where θ is the model parameters, and N denotes the number of categories in the target domain.

3.2. A Frequency Causal View for DG

To gain deeper insights into the relationship between the Fourier spectra and DG, we initially consider domain generalization as a domain-specific image generation task from a causal perspective. As depicted in Fig. 2a, given information about an *object* (O) and a *domain* (D), we generate a domain-specific image X with its corresponding category label Y . The image generating process first samples O and D , which are mutually independent. The pixels of the image X are then constructed using the latent embeddings of both O and D , whereas the category label Y is solely influenced by O . In this context, we consider the latent embeddings caused by O and D as causal factors (C) and non-causal factors (N), respectively.

Based on Reichenbach’s *Common Cause Principle* [41], the SCM of domain-specific image generation process can be formulated as follows:

$$\begin{aligned} C &= U_O, N = U_D, \\ X &= g_x(C, N; \theta) + U_X, \\ Y &= g_y(C; \theta) + U_Y, \end{aligned} \quad (2)$$

where $U = \{U_O, U_D, U_X, U_Y\}$ denotes the *exogenous variables*, and $V = \{X, Y, C, N\}$ denotes the *endogenous variables*. Note that C and N satisfy the following conditions: **(1)** $C \not\perp\!\!\!\perp O, N \not\perp\!\!\!\perp D$; **(2)** $C \perp\!\!\!\perp D | O, N \perp\!\!\!\perp O | D$. The latter condition ensures that C is invariant with the same object across different domains, and N is independent of the object. Unfortunately, due to the unobservation of causal/non-causal factors, we cannot directly formulate $X = g_x(C, N; \theta) + U_X$, which remains a challenging problem for causal inference [8] and poses a further obstacle to modeling the distribution from X to Y .

Based on our observation in Sec. 1 and the well-known property of Fourier transform: The phase spectrum preserves high-level semantics of the image while the amplitude spectrum contains low-level statistics [12, 29, 35, 36, 51, 52]. We believe that introducing Fourier transform into causal inference might help learn causal representations. Hence, with reference to [3], we make the following assumption for components of the Fourier transform:

Assumption 1 *The phase component of the Fourier spectrum is dependent on both the object and domain information. The amplitude component is only dependent on the domain information.*

With Assumption 1, we can have a formal statement for the generation process:

Corollary 1 *The category label of the generated image is only dependent on the phase spectrum, the pixels of the image is constructed from both the phase and amplitude spectrum.*

The proof is omitted because Corollary 1 has been empirically verified in Sec. 1 and previous work [3]. Therefore the corollary can serve as the causal explanation to generalizability of CNN in DG.

With Corollary 1, we treat the phase spectrum \mathcal{P} as the semi-causal factors (note that a causal relation between domain (D) and the phase spectrum (\mathcal{P}) is introduced) and the amplitude spectrum \mathcal{A} as the redundant non-causal factors. We transform the general form Eq. (2) to the following specified form (depicted in Fig. 2b):

$$\begin{aligned} \mathcal{P} &= U_O + U_D, \mathcal{A} = U_D, \\ X &= g_x(\mathcal{P}, \mathcal{A}; \theta) + U_X, \\ Y &= g_y(\mathcal{P}; \theta) + U_Y. \end{aligned} \quad (3)$$

Here, we present an intuitive view of the Structural Causal Model (SCM) of the human visual system from the frequency perspective. By having access to the factors in causal inference, we can perform operations on the specified factors instead of blindly exploring the highly-entangled latent space. As the amplitude spectrum has no

association with the category label, reducing or even eliminating its impact can significantly improve the Signal-to-Noise Ratio (SNR) of the image, thereby aiding the model in learning the intrinsic features of objects.

3.3. Phase Match

From the above perspective, Domain Generalization (DG) can be viewed as a process of generating domain-specific images, where the phase spectrum of the image is considered the *semi-causal factors*. Our hypothesis is that a robust representation remains invariant to the phase spectrum of the object despite significant perturbations in the amplitude spectrum. Based on this motivation, we introduce Phase Match, as described next.

3.3.1 Data Augmentation with Amplitude Perturbation

As is discussed in Sec. 1 and Sec. 3.2, the network is vulnerable to the amplitude perturbations, which is usually caused by domain shifts. To make the network robust to this perturbation, an intuitive way is to add attacks for the training examples to get adversarial gradients. Considering the semantic-preserving property of Fourier phase spectrum [35, 36, 39], we introduce perturbations upon the amplitude information by linearly interpolating between the amplitude spectrums of two randomly-sampled images, while maintaining the phase spectrums unchanged as in [29, 51].

Formally, given an image $x \in \mathbb{R}^{H \times W \times 3}$, we can obtain the complex spectrum $\mathcal{F} \in \mathbb{C}^{H \times W \times 3}$ computed across the spatial dimension within each channel by FFT [34]:

$$\mathcal{F}(x)(u, v) = \sum_{h=0}^{H-1} \sum_{w=0}^{W-1} x(h, w) \cdot e^{-j2\pi(\frac{h}{H}u + \frac{w}{W}v)}, \quad (4)$$

where H and W represent the height and width of the image respectively.

We then perturb the amplitude components of two images x_o, x'_o from arbitrary source domains by the way as MixUP [57]:

$$\hat{\mathcal{A}}_o' = (1 - \lambda)\mathcal{A}(x_o) + \lambda\mathcal{A}(x'_o), \quad (5)$$

where $\lambda \sim U(0, \eta)$ and η is a hyperparameter which controls the scale of perturbation. The phase-invariant image x_a is then generated from the combination of original phase component and mixed amplitude component:

$$x_a = \mathcal{F}^{-1}(\hat{\mathcal{A}}_o' \otimes e^{-j \cdot \mathcal{P}(x_o)}). \quad (6)$$

The augmented image pairs and the corresponding original labels are both fed to the model for training. The prediction loss is formulated as the standard Cross Entropy Loss:

$$\mathcal{L}_{cls}^{o(a)} = -y^T \log(\sigma(g(x_{o(a)}; \theta))), \quad (7)$$

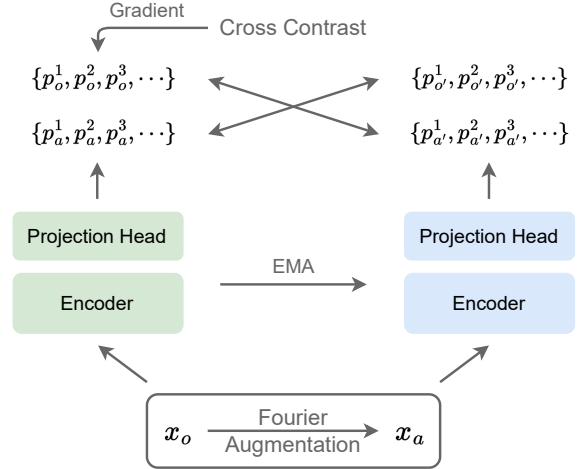


Figure 3. Framework of PhaMa. The Fourier-augmented image pairs (x_o and x_a) are both fed to the encoder and the momentum-updated encoder, then, the last-two-level features are sent to a 2-layer nonlinear projection head for extracting patch representations $p_{o(a)}^i$. The cross contrastive gradients are backpropagated for updating the encoder and projection head (greens); for the momentums (blues), parameters are updated by EMA.

where σ denotes the *softmax* function.

By leveraging this simple operation, we enhance the network’s robustness to unknown amplitude shifts. Importantly, since the phase component remains intact during this operation, we effectively build positive pairs, which, in turn, paves the way for our subsequent contrastive regularization to improve the network’s ability to capture the phase features.

3.3.2 Matching Phase with Cross Patch Contrast

At the core of our method is *matching* the phase component of the original image with the corresponding augmented sample; in other words, the representation of the image pairs should exhibit similarity or even be the same. Our research reveals that there is currently no neural network-based method that specifically focuses on extracting phase spectrum features. Consequently, we face challenges in directly matching the phase embeddings with common metrics such as L1, L2, KLD. To address this, we incorporate contrastive learning [11], an unsupervised learning method that measures the similarities of sample pairs in a representation space, into our method.

Given the encoded hierarchal feature maps of an image $f_j(x)$, where j denotes the index of the feature map, e.g., for a ResNet-like network, $j \in \{1, 2, 3, 4\}$. Our choice of the feature representations is the *last-two-levels* in a hierarchal network, in that the high-level features of the network are more tend to extract semantic-related informa-

tion [56]. Specifically, for the two hierarchical representations $f_3 \in \mathbb{R}^{C_3 \times H_3 \times W_3}$ and $f_4 \in \mathbb{R}^{C_4 \times H_4 \times W_4}$, we resize f_4 by bilinear interpolation and concatenate them in the channel dimension, denoted as z , and send them to a 2-layer nonlinear projection head $p(z) = W_1 \sigma(W_2 z)$ as in [4].

Inspired by the high consistency of the phase spectrum in preserving spatial structures, *i.e.*, for the same position in the image pairs in Sec. 1, contours and edges are highly consistent. We aim to establish associations for each patch in the spatial dimension, *i.e.*, make the patch representations from the same location *similar*, and *push away* those from different positions as far as possible. In this way, the encoded representations from each patch are consistent under the amplitude perturbation, and the network can learn from the invariant phase spectrum. Therefore, the following PatchNCE loss [37] is considered:

$$\mathcal{L}_{patch}^{o2a'} = - \sum_i \log \frac{\exp(p_o^i \cdot p_{a'}^i / \tau)}{\exp(p_o^i \cdot p_{a'}^i / \tau) + \sum_j \exp(p_o^i \cdot p_{a'}^j / \tau)}, \quad (8)$$

where p_o and $p_{a'}$ are from the encoder and the momentum encoder respectively, $i(j) \in \{1, \dots, P\}$ denotes the index of the patch, (\cdot) denotes the inner product, τ is a temperature parameter. For the i th patch in the original image p_o^i , patches in other location in the augmented image $p_{a'}^j (j \neq i)$ are treated as negative samples, the contrast can then be set as a P -way classification problem (Fig. 4).

However, existing pre-trained networks [6, 15] extract very different representations (Sec. 1) under huge perturbations of amplitude information, which tends to cause gradient collapsing during the back-propagation in our experiments (Sec. 4.3). To alleviate the impact caused by amplitude perturbations:

- For both the original and augmented images, we adopt a momentum-updated encoder to ensure consistent representation extraction, following the approach proposed in [14]. Specifically, we update the parameters of the encoder, denoted as θ , and the momentum encoder, denoted as θ_m , using the following update rule:

$$\theta_m \leftarrow m\theta_m + (1 - m)\theta. \quad (9)$$

- We perform the patch contrast operation (Eq. (8)) *across* the patch representation of the original image and the augmented from the encoder and the momentum encoder, respectively. The contrastive loss is defined as:

$$\mathcal{L}_{contr} = \mathcal{L}_{patch}^{o2a'} + \mathcal{L}_{patch}^{a2o'}. \quad (10)$$

The overall objective function of our proposed method can be formulated as follows:

$$\mathcal{L}_{PhaMa} = \frac{1}{2}(\mathcal{L}_{cls}^o + \mathcal{L}_{cls}^a) + \beta \mathcal{L}_{contr}, \quad (11)$$

where β is a trade-off parameter.

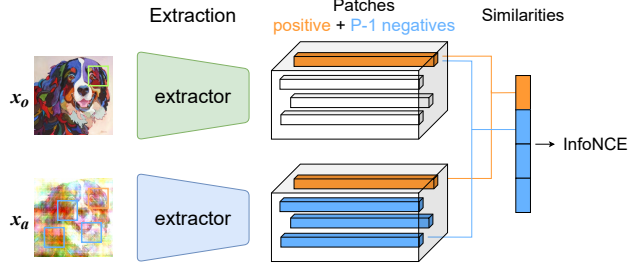


Figure 4. Illustration of PatchNCE loss.

4. Experiment

In this section, we conduct experiments on several benchmarks to evaluate the effectiveness of our method in improving generalization ability of networks, including multi-domain classification and robustness towards corruptions. More details about the implementation, results analysis and ablation studies will be discussed in the following.

4.1. Multi-domain Classification

4.1.1 Implementation Details

Datasets. We evaluate the generalization ability of our method on the following 3 datasets: (1)**Digits-DG** [60], consisting of four datasets MNIST [23], MNIST-M [7], SVHN [32], SYN [7]; (2)**PACS** [24], a commonly used benchmark for domain generalization, comprising of 9991 images from four distinct domains: Art Painting, Cartoon, Photo, Sketch; (3)**Office-Home** [46], which contains around 15,500 images of 65 categories from four domains: Artistic, Clipart, Product and Real World.

Training. For all DG benchmarks, we follow the leave-one-domain-out protocol with official train-val split, and report the classification accuracy (%) on the entire held-out target domain. We also use the standard augmentation, which consists of random resized cropping, horizontal flipping and color jittering. For Digits-DG, all images are resized to 32×32 . We train the encoder (same as in [60]) from scratch using SGD, batch size 64 and weight decay of $5e-4$, the learning rate is initially 0.05 and is decayed by 0.1 every 20 epochs. For PACS and Office-Home, all images are resized to 224×224 . We use the ImageNet pre-trained ResNet [15] as the encoder, and train the network with SGD, batch size 64, momentum 0.9 and weight decay $5e-4$ for 50 epochs. The initial learning rate is 0.001 and decayed by 0.1 at 80% of the total epochs.

Method-specific. We use a sigmoid ramp-up [43] for β within first 5 epochs in all experiments. The trade-off parameter β is set to 0.1 for Digits-DG, and 0.5 for PACS and Office-Home. We also follow the common setting [49] to let $\tau = 0.07$.

Table 1. Leave-one-domain-out classification accuracy (%) on Digits-DG.

Method	MNIST	MNIST-M	SVHN	SYN	Avg.
Baseline	95.8	58.8	61.7	78.6	73.7
CCSA	95.2	58.2	65.5	79.1	74.5
MMD-AAE	96.5	58.4	65.0	78.4	74.6
CrossGrad	96.7	61.1	65.3	80.2	75.8
DDAIG	96.6	64.1	68.6	81.0	77.6
Jigen	96.5	61.4	63.7	74.0	73.9
L2A-OT	96.7	63.9	68.6	83.2	78.1
MixStyle	96.5	63.5	64.7	81.2	76.5
FACT	96.8	63.2	73.6	89.3	80.7
PhaMa (<i>ours</i>)	97.3	63.9	73.2	90.2	81.1

Table 2. Leave-one-domain-out classification accuracy (%) on PACS with ResNet pretrained on ImageNet.

Method	Art	Cartoon	Photo	Sketch	Avg.
ResNet-18					
Baseline	77.6	76.7	95.8	69.5	79.9
MixUP	76.8	74.9	95.8	66.6	78.5
CutMix	74.6	71.8	95.6	65.3	76.8
pAdaIN	81.7	76.6	96.3	75.1	82.5
MixStyle	82.3	79.0	96.3	73.8	82.8
DSU	83.6	79.6	95.8	77.6	84.1
MetaReg	83.7	77.2	95.5	70.3	81.7
JiGen	79.4	75.2	96.0	71.3	80.5
MASF	80.2	77.1	94.9	71.6	81.1
L2A-OT	83.3	78.0	96.2	73.6	82.8
RSC (<i>our imp.</i>)	80.5	78.6	94.4	76.0	82.4
MatchDG	81.3	80.7	96.5	79.7	84.5
SelfReg	82.3	78.4	96.2	77.4	83.6
FACT	85.3	78.3	95.1	79.1	84.5
PhaMa (<i>ours</i>)	84.8	79.1	96.6	79.7	85.1
ResNet-50					
Baseline	84.9	76.9	97.6	76.7	84.1
MetaReg	87.2	79.2	97.6	70.3	83.6
MASF	82.8	80.4	95.0	72.2	82.7
RSC (<i>our imp.</i>)	83.9	79.5	95.1	82.2	85.2
MatchDG	85.6	82.1	97.9	78.7	86.1
FACT	89.6	81.7	96.7	84.4	88.1
PhaMa (<i>ours</i>)	89.6	82.7	97.2	83.7	88.3

Model Selection. We use training-domain validation set for model selection. Specifically, we train our model on the training splits of all source domains and choose the model maximizing the accuracy on the overall validation set.

Table 3. Leave-one-domain-out classification accuracy (%) on Office-Home with ResNet-18 pretrained on ImageNet.

Method	Art	Clipart	Product	Real	Avg.
Baseline	57.8	52.7	73.5	74.8	64.7
CCSA	59.9	49.9	74.1	75.7	64.9
MMD-AAE	56.5	47.3	72.1	74.8	62.7
CrossGrad	58.4	49.4	73.9	75.8	64.4
DDAIG	59.2	52.3	74.6	76.0	65.5
L2A-OT	60.6	50.1	74.8	77.0	65.6
Jigen	53.0	47.5	71.4	72.7	61.2
MixStyle	58.7	53.4	74.2	75.9	65.5
DSU	60.2	54.8	74.1	75.1	66.1
FACT	60.3	54.8	74.4	76.5	66.5
PhaMa (<i>ours</i>)	60.2	54.0	75.2	76.4	66.5

4.1.2 Results Analysis

Digits-DG. Results are shown in Tab. 1. PhaMa achieves great improvement over the baseline method and surpasses previous domain-invariant methods by a large margin. Since our method adopts the same augmentation technique as FACT [51], we compare our method with it. Our method shows slight improvement over FACT, which means that matching the patch feature is more suitable for cross-domain representation.

PACS. The experimental results presented in Tab. 2 show a significant improvement of our PhaMa method compared to the baseline approach. Particularly, PhaMa exhibits substantial improvements in average accuracy, notably in Art, Cartoon, and Sketch domains. It is worth noting that previous DG methods tend to experience a slight drop in accuracy for the Photo domain, which shares similar domain characteristics with the ImageNet dataset, and this drop might be attributed to ImageNet pretraining. However, our method is capable of either maintaining or lifting the performance in the Photo domain, demonstrating that contrasting phase components does not degrade raw representations.

Note that other contrast-based methods such as MatchDG and SelfReg also demonstrate competitive performance on Photo and other domains. This observation highlights the effectiveness of contrastive learning as a powerful tool for DG. Meanwhile, the exceptional performance of our PhaMa method suggests that introducing spatial contrast for the phase component can yield even more promising results.

Office-Home. Results are shown in Tab. 3. It can be observed that our method brings obvious improvement over the baseline method and also achieves competitive results against FACT. By introducing the amplitude perturbation and patch contrastive loss, the model can learn to alleviate

Table 4. Mean Corruption Error (%) on CIFAR-10(100)-C.

Arch. Method	ResNet	DenseNet	WideResNet	ResNeXt
CIFAR-10-C				
Standard	-	30.7	26.9	27.5
Cutout	-	32.1	26.8	28.9
MixUP	-	24.6	22.3	22.6
CutMix	-	33.5	27.1	29.5
Adv Training	-	27.6	26.2	27.0
APR	16.7	20.3	18.3	18.5
PhaMa (<i>ours</i>)	17.5	20.3	17.5	17.9
CIFAR-100-C				
Standard	-	59.3	53.3	53.4
Cutout	-	59.6	53.5	54.6
MixUP	-	55.4	50.4	51.4
CutMix	-	59.2	52.9	54.1
Adv Training	-	55.2	55.1	54.4
APR	43.8	49.8	44.7	44.2
PhaMa (<i>ours</i>)	43.8	48.5	43.9	41.5

the amplitude impacts and focus on the phase information.

4.2. Robustness Towards Corruptions

4.2.1 Implementation Details

Datasets. We evaluate the robustness towards corruptions of our method on CIFAR-10-C, CIFAR-100-C [16]. The two datasets are constructed by corrupting the test split of original CIFAR dataset with a total of 15 corruption types (*noise, blur, weather* and *digital*). Note that the 15 corruptions are not introduced in training.

Training. Following [3], we evaluate our method on various architectures of networks, including ResNet-18 [15], 40-2 Wide-ResNet [55], DenseNet-BC ($k = 2, d = 100$) [18], and ResNeXt-29 (32×4) [50]. All networks use an initial learning rate of 0.1 which decay every 60 epochs. We train all models from scratch for 200 epochs using SGD, batch size 128, momentum 0.9. All input images are randomly processed with resized cropping and horizontal flipping.

Method-specific. All configurations are in line with Sec. 4.1.1.

Model Selection. We select the last-epoch model for evaluations on corrupted datasets.

4.2.2 Results Analysis

We present the mean Corruption Error (%) for CIFAR-10-C and CIFAR-100-C in Tab. 4. Our PhaMa method outperforms conventional data augmentation techniques (Cutout, MixUP, CutMix) by a significant margin. Furthermore, PhaMa shows slight improvements over APR, which also

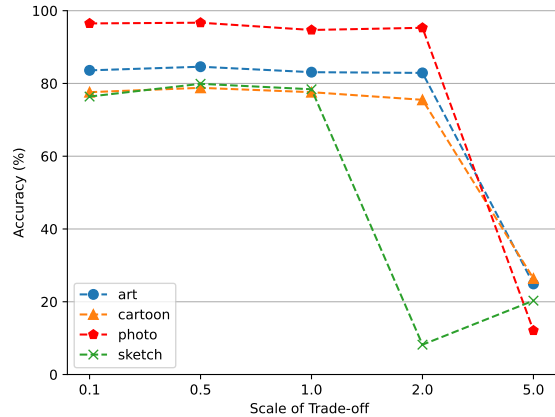


Figure 5. Evaluation of different trade-off parameters.

employs a similar technique in the frequency domain like ours. This observation demonstrates that building spatial relationships for the phase information can further enhance the extraction of intrinsic representations by the model.

4.3. Ablation Studies

Effects of Different Modules. We conduct ablation studies to investigate the impact of each module in our method in Tab. 5. Compared with baseline, the amplitude perturbation data augmentation module (APDA) plays a significant role in our method, which lifts the performance by a margin of 4.5%. We exclude the momentum-updated encoder (MoEnc) for variant B, and the performance drops by nearly 1%, demonstrating the network’s over-dependence on the amplitude spectrum makes the feature extraction inefficient. With the cross contrast operation for the image pairs, PhaMa surpasses variant C and D, suggesting that keeping the consistency between the image pairs is important for the training of contrastive learning.

Sensitivity of Trade-off Parameter. The hyperparameter β controls the trade-off between the classification loss and the patch contrastive loss. We experiment with different values of β from the set $\{0, 0.1, 0.5, 1.0, 2.0, 5.0\}$. The results, depicted in Fig. 5, show that for small β values, there are slight oscillations in the results. However, when β is set to a large value, the training process collapses. We hypothesize that the collapse is attributed to an over-dependence on the amplitude spectrum of the ImageNet pretrained weights. As β increases, the intense contrast objective tends to corrupt the raw representation.

Choices of Match Loss. Since our objective is to match the representation of each patch from the image pairs, we evaluate various types of matching loss, including SmoothL1, MSE, and PatchNCE. As demonstrated in Tab. 6, the Patch-

Table 5. Effects of different modules on PACS with ResNet-18.

Method	APDA	$\mathcal{L}_{patch}^{o2a}$	$\mathcal{L}_{patch}^{a2o}$	MoEnc	Art	Cartoon	Photo	Sketch	Avg.
Baseline	-	-	-	-	77.6	76.7	95.8	69.5	79.9
Variant A	✓	-	-	-	83.9	76.9	95.5	77.6	83.4
Variant B	✓	✓	✓	-	83.2	77.1	95.5	79.0	83.7
Variant C	✓	✓	-	✓	84.2	78.7	96.1	79.5	84.6
Variant D	✓	-	✓	✓	84.1	78.4	95.5	79.1	84.5
PhaMa	✓	✓	✓	✓	84.8	79.1	96.6	79.7	85.1

Table 6. Evaluation of different types of matching loss.

Type	Art	Cartoon	Photo	Sketch	Avg.
SmoothL1	83.7	76.6	96.4	72.3	82.3
MSE	81.8	77.4	96.6	76.1	83.0
PatchNCE	84.8	79.1	96.6	79.7	85.1

Table 7. Average Accuracy (%) and GPU Memory-Usage (GB) of different positions.

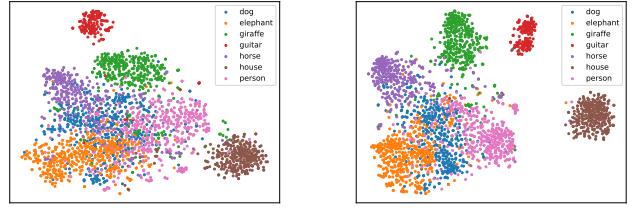
Position	Avg Acc	Mem-Usage
1, 2	82.2	~43.3
2, 3	83.5	~12.1
3, 4	85.1	~11.8

NCE loss outperforms the others on Art Painting, Cartoon, and Sketch domains, while also showing competitive performance on the Photo domain. The inferior performance of SmoothL1 and MSE losses is likely attributed to the simplistic alignment of the representation, which lacks weighting to enable the network to effectively discriminate the positive patch from the others.

Impacts of Hierarchies. Table 7 compares different hierarchical positions (indexed with 1-4) in the ResNet bolcks for contrastive learning. As can be seen, the representation extracted from the last two layers occupies the least GPU memory while achieving the best effect performance.

4.4. Visualization

To intuitively present PhaMa’s effects on feature representations, we visualize the feature representation vectors of different categories in unseen domain with t-SNE [45] in Fig. 6. Compared with baseline method, features from the same category become more compact with our method. The clustered representations illustrate that our method can alleviate perturbations caused by domain shifts and extract more domain-invariant features.



(a) Baseline.

(b) PhaMa.

Figure 6. t-SNE visualization on Baseline and proposed PhaMa. We visualize the embeddings of ResNet-18 on PACS benchmark with art, photo and sketch as the source domains, and cartoon as the target domain.

5. Discussion and Conclusion

In this paper, we consider DG from a frequency perspective and present PhaMa. The main idea is establishing spatial relationships for the phase spectrum. Our method shows promising results of introducing spatial relationships for phase information on many DG benchmarks.

Moreover, several questions are worth rethinking. Even though the cross-domain impact of amplitude information is alleviated, our method doesn’t actually build relationships between cross-domain samples, *i.e.*, the intrinsic domain-invariant representation learning is still weakly reflected. As shown in Fig. 6, minority features are still outliers from the cluster. The above limitations might result in the slight improvement of PhaMa on many DG benchmarks. Beyond domain generalization, PhaMa draws on MoCo [14] for many module designs. Considering the great property of the Fourier transform, it is worth thinking that (1) can the phase information be a prior embedding, *e.g.*, position embedding in Transformer [45], to augment the original visual signal, (2) whether the Fourier transform and the spatial relationship of the phase spectrum can be extended to unsupervised visual representation learning or even multimodal learning [40]. We hope our work can bring more inspirations into the community.

References

- [1] Martin Arjovsky, Léon Bottou, Ishaan Gulrajani, and David Lopez-Paz. Invariant risk minimization. *arXiv preprint arXiv:1907.02893*, 2019. 1
- [2] Mathilde Caron, Hugo Touvron, Ishan Misra, Hervé Jégou, Julien Mairal, Piotr Bojanowski, and Armand Joulin. Emerging properties in self-supervised vision transformers. In *Proceedings of the IEEE/CVF international conference on computer vision*, pages 9650–9660, 2021. 2
- [3] Guangyao Chen, Peixi Peng, Li Ma, Jia Li, Lin Du, and Yonghong Tian. Amplitude-phase recombination: Rethinking robustness of convolutional neural networks in frequency domain. In *Proceedings of the IEEE/CVF International Conference on Computer Vision*, pages 458–467, 2021. 1, 2, 3, 7
- [4] Ting Chen, Simon Kornblith, Mohammad Norouzi, and Geoffrey Hinton. A simple framework for contrastive learning of visual representations. In *International conference on machine learning*, pages 1597–1607. PMLR, 2020. 2, 5
- [5] Jia Deng, Wei Dong, Richard Socher, Li-Jia Li, Kai Li, and Li Fei-Fei. Imagenet: A large-scale hierarchical image database. In *2009 IEEE conference on computer vision and pattern recognition*, pages 248–255. Ieee, 2009. 1
- [6] Alexey Dosovitskiy, Lucas Beyer, Alexander Kolesnikov, Dirk Weissenborn, Xiaohua Zhai, Thomas Unterthiner, Mostafa Dehghani, Matthias Minderer, Georg Heigold, Sylvain Gelly, Jakob Uszkoreit, and Neil Houlsby. An image is worth 16x16 words: Transformers for image recognition at scale. *ICLR*, 2021. 2, 5
- [7] Yaroslav Ganin and Victor Lempitsky. Unsupervised domain adaptation by backpropagation. In *International conference on machine learning*, pages 1180–1189. PMLR, 2015. 5
- [8] Andrew Gelman. Causality and statistical learning, 2011. 3
- [9] Ian Goodfellow, Yoshua Bengio, and Aaron Courville. *Deep learning*. MIT press, 2016. 1
- [10] Chuan Guo, Jared S Frank, and Kilian Q Weinberger. Low frequency adversarial perturbation. *arXiv preprint arXiv:1809.08758*, 2018. 1, 2
- [11] Raia Hadsell, Sumit Chopra, and Yann LeCun. Dimensionality reduction by learning an invariant mapping. In *2006 IEEE Computer Society Conference on Computer Vision and Pattern Recognition (CVPR'06)*, volume 2, pages 1735–1742. IEEE, 2006. 2, 4
- [12] Bruce C Hansen and Robert F Hess. Structural sparseness and spatial phase alignment in natural scenes. *JOSA A*, 24(7):1873–1885, 2007. 3
- [13] Kaiming He, Xinlei Chen, Saining Xie, Yanghao Li, Piotr Dollár, and Ross Girshick. Masked autoencoders are scalable vision learners. In *Proceedings of the IEEE/CVF conference on computer vision and pattern recognition*, pages 16000–16009, 2022.
- [14] Kaiming He, Haoqi Fan, Yuxin Wu, Saining Xie, and Ross Girshick. Momentum contrast for unsupervised visual representation learning. In *Proceedings of the IEEE/CVF conference on computer vision and pattern recognition*, pages 9729–9738, 2020. 2, 5, 8
- [15] Kaiming He, Xiangyu Zhang, Shaoqing Ren, and Jian Sun. Deep residual learning for image recognition. In *Proceedings of the IEEE conference on computer vision and pattern recognition*, pages 770–778, 2016. 1, 5, 7
- [16] Dan Hendrycks and Thomas Dietterich. Benchmarking neural network robustness to common corruptions and perturbations. *Proceedings of the International Conference on Learning Representations*, 2019. 7
- [17] Dan Hendrycks, Norman Mu, Ekin D Cubuk, Barret Zoph, Justin Gilmer, and Balaji Lakshminarayanan. Augmix: A simple data processing method to improve robustness and uncertainty. *arXiv preprint arXiv:1912.02781*, 2019. 1
- [18] Gao Huang, Zhuang Liu, Laurens Van Der Maaten, and Kilian Q Weinberger. Densely connected convolutional networks. In *Proceedings of the IEEE conference on computer vision and pattern recognition*, pages 4700–4708, 2017. 7
- [19] Xun Huang and Serge Belongie. Arbitrary style transfer in real-time with adaptive instance normalization. In *Proceedings of the IEEE international conference on computer vision*, pages 1501–1510, 2017. 1, 2
- [20] Maximilian Ilse, Jakub M Tomczak, Christos Louizos, and Max Welling. Diva: Domain invariant variational autoencoders. In *Medical Imaging with Deep Learning*, pages 322–348. PMLR, 2020. 1
- [21] Daehee Kim, Youngjun Yoo, Seunghyun Park, Jinkyu Kim, and Jaekoo Lee. Selfreg: Self-supervised contrastive regularization for domain generalization. In *Proceedings of the IEEE/CVF International Conference on Computer Vision*, pages 9619–9628, 2021. 2
- [22] Yann LeCun, Yoshua Bengio, and Geoffrey Hinton. Deep learning. *nature*, 521(7553):436–444, 2015. 1
- [23] Yann LeCun, Léon Bottou, Yoshua Bengio, and Patrick Haffner. Gradient-based learning applied to document recognition. *Proceedings of the IEEE*, 86(11):2278–2324, 1998. 5
- [24] Da Li, Yongxin Yang, Yi-Zhe Song, and Timothy M Hospedales. Deeper, broader and artier domain generalization. In *Proceedings of the IEEE international conference on computer vision*, pages 5542–5550, 2017. 5
- [25] Haoliang Li, Sinno Jialin Pan, Shiqi Wang, and Alex C Kot. Domain generalization with adversarial feature learning. In *Proceedings of the IEEE conference on computer vision and pattern recognition*, pages 5400–5409, 2018. 1, 2
- [26] Lei Li, Ke Gao, Juan Cao, Ziyao Huang, Yepeng Weng, Xiaoyue Mi, Zhengze Yu, Xiaoya Li, and Boyang Xia. Progressive domain expansion network for single domain generalization. In *Proceedings of the IEEE/CVF Conference on Computer Vision and Pattern Recognition*, pages 224–233, 2021. 2
- [27] Xiaotong Li, Yongxing Dai, Yixiao Ge, Jun Liu, Ying Shan, and LINGYU DUAN. Uncertainty modeling for out-of-distribution generalization. In *International Conference on Learning Representations*, 2022. 1, 2
- [28] Honggu Liu, Xiaodan Li, Wenbo Zhou, Yuefeng Chen, Yuan He, Hui Xue, Weiming Zhang, and Nenghai Yu. Spatial-phase shallow learning: rethinking face forgery detection in frequency domain. In *Proceedings of the IEEE/CVF con-*

- ference on computer vision and pattern recognition*, pages 772–781, 2021. [1](#)
- [29] Fangrui Lv, Jian Liang, Shuang Li, Bin Zang, Chi Harold Liu, Ziteng Wang, and Di Liu. Causality inspired representation learning for domain generalization. In *Proceedings of the IEEE/CVF Conference on Computer Vision and Pattern Recognition*, pages 8046–8056, 2022. [1](#), [2](#), [3](#), [4](#)
- [30] Divyat Mahajan, Shruti Tople, and Amit Sharma. Domain generalization using causal matching. In *International Conference on Machine Learning*, pages 7313–7324. PMLR, 2021. [1](#)
- [31] Krikamol Muandet, David Balduzzi, and Bernhard Schölkopf. Domain generalization via invariant feature representation. In *International conference on machine learning*, pages 10–18. PMLR, 2013. [1](#)
- [32] Yuval Netzer, Tao Wang, Adam Coates, Alessandro Bisacco, Bo Wu, and Andrew Y. Ng. Reading digits in natural images with unsupervised feature learning. In *NIPS Workshop on Deep Learning and Unsupervised Feature Learning 2011*, 2011. [5](#)
- [33] Oren Nuriel, Sagie Benaim, and Lior Wolf. Permuted adain: Reducing the bias towards global statistics in image classification. In *Proceedings of the IEEE/CVF Conference on Computer Vision and Pattern Recognition*, pages 9482–9491, 2021. [1](#), [2](#)
- [34] Henri J Nussbaumer and Henri J Nussbaumer. *The fast Fourier transform*. Springer, 1981. [4](#)
- [35] A Oppenheim, Jae Lim, Gary Kopec, and SC Pohlig. Phase in speech and pictures. In *ICASSP’79. IEEE International Conference on Acoustics, Speech, and Signal Processing*, volume 4, pages 632–637. IEEE, 1979. [3](#), [4](#)
- [36] Alan V Oppenheim and Jae S Lim. The importance of phase in signals. *Proceedings of the IEEE*, 69(5):529–541, 1981. [3](#), [4](#)
- [37] Taesung Park, Alexei A Efros, Richard Zhang, and Jun-Yan Zhu. Contrastive learning for unpaired image-to-image translation. In *Computer Vision—ECCV 2020: 16th European Conference, Glasgow, UK, August 23–28, 2020, Proceedings, Part IX 16*, pages 319–345. Springer, 2020. [2](#), [5](#)
- [38] Xingchao Peng, Zijun Huang, Ximeng Sun, and Kate Saenko. Domain agnostic learning with disentangled representations. In *International Conference on Machine Learning*, pages 5102–5112. PMLR, 2019. [1](#), [2](#)
- [39] Leon N Piotrowski and Fergus W Campbell. A demonstration of the visual importance and flexibility of spatial-frequency amplitude and phase. *Perception*, 11(3):337–346, 1982. [4](#)
- [40] Alec Radford, Jong Wook Kim, Chris Hallacy, Aditya Ramesh, Gabriel Goh, Sandhini Agarwal, Girish Sastry, Amanda Askell, Pamela Mishkin, Jack Clark, et al. Learning transferable visual models from natural language supervision. In *International conference on machine learning*, pages 8748–8763. PMLR, 2021. [8](#)
- [41] Maria Reichenbach and P Morrison. The direction of time. *Physics Today*, 9(10):24–28, 1956. [3](#)
- [42] Yash Sharma, Gavin Weiguang Ding, and Marcus Brubaker. On the effectiveness of low frequency perturbations. page 3389–3396, 2019. [1](#), [2](#)
- [43] Antti Tarvainen and Harri Valpola. Mean teachers are better role models: Weight-averaged consistency targets improve semi-supervised deep learning results. *Advances in neural information processing systems*, 30, 2017. [5](#)
- [44] Dmitry Ulyanov, Andrea Vedaldi, and Victor Lempitsky. Instance normalization: The missing ingredient for fast stylization. *arXiv preprint arXiv:1607.08022*, 2016. [2](#)
- [45] Laurens Van der Maaten and Geoffrey Hinton. Visualizing data using t-sne. *Journal of machine learning research*, 9(11), 2008. [8](#)
- [46] Hemanth Venkateswara, Jose Eusebio, Shayok Chakraborty, and Sethuraman Panchanathan. Deep hashing network for unsupervised domain adaptation. In *Proceedings of the IEEE conference on computer vision and pattern recognition*, pages 5018–5027, 2017. [5](#)
- [47] Haohan Wang, Xindi Wu, Zeyi Huang, and Eric P Xing. High-frequency component helps explain the generalization of convolutional neural networks. In *Proceedings of the IEEE/CVF conference on computer vision and pattern recognition*, pages 8684–8694, 2020. [1](#), [2](#)
- [48] Jindong Wang, Cuiling Lan, Chang Liu, Yidong Ouyang, Tao Qin, Wang Lu, Yiqiang Chen, Wenjun Zeng, and Philip Yu. Generalizing to unseen domains: A survey on domain generalization. *IEEE Transactions on Knowledge and Data Engineering*, 2022. [2](#)
- [49] Zhirong Wu, Yuanjun Xiong, Stella X Yu, and Dahua Lin. Unsupervised feature learning via non-parametric instance discrimination. In *Proceedings of the IEEE conference on computer vision and pattern recognition*, pages 3733–3742, 2018. [2](#), [5](#)
- [50] Saining Xie, Ross Girshick, Piotr Dollár, Zhuowen Tu, and Kaiming He. Aggregated residual transformations for deep neural networks. In *Proceedings of the IEEE conference on computer vision and pattern recognition*, pages 1492–1500, 2017. [7](#)
- [51] Qinwei Xu, Ruipeng Zhang, Ya Zhang, Yanfeng Wang, and Qi Tian. A fourier-based framework for domain generalization. In *Proceedings of the IEEE/CVF Conference on Computer Vision and Pattern Recognition*, pages 14383–14392, 2021. [2](#), [3](#), [4](#), [6](#)
- [52] Yanchao Yang and Stefano Soatto. Fda: Fourier domain adaptation for semantic segmentation. In *Proceedings of the IEEE/CVF Conference on Computer Vision and Pattern Recognition*, pages 4085–4095, 2020. [3](#)
- [53] Xufeng Yao, Yang Bai, Xinyun Zhang, Yuechen Zhang, Qi Sun, Ran Chen, Ruiyu Li, and Bei Yu. Pcl: Proxy-based contrastive learning for domain generalization. In *Proceedings of the IEEE/CVF Conference on Computer Vision and Pattern Recognition*, pages 7097–7107, 2022. [2](#)
- [54] Sangdoo Yun, Dongyoon Han, Seong Joon Oh, Sanghyuk Chun, Junsuk Choe, and Youngjoon Yoo. Cutmix: Regularization strategy to train strong classifiers with localizable features. In *Proceedings of the IEEE/CVF International Conference on Computer Vision (ICCV)*, October 2019. [1](#), [2](#)
- [55] Sergey Zagoruyko and Nikos Komodakis. Wide residual networks. *arXiv preprint arXiv:1605.07146*, 2016. [7](#)

- [56] Matthew D Zeiler and Rob Fergus. Visualizing and understanding convolutional networks. In *Computer Vision–ECCV 2014: 13th European Conference, Zurich, Switzerland, September 6–12, 2014, Proceedings, Part I 13*, pages 818–833. Springer, 2014. 5
- [57] Hongyi Zhang, Moustapha Cisse, Yann N. Dauphin, and David Lopez-Paz. mixup: Beyond empirical risk minimization. In *International Conference on Learning Representations*, 2018. 1, 2, 4
- [58] Shanshan Zhao, Mingming Gong, Tongliang Liu, Huan Fu, and Dacheng Tao. Domain generalization via entropy regularization. In *Advances in Neural Information Processing Systems*, volume 33, pages 16096–16107, 2020. 2
- [59] Kaiyang Zhou, Ziwei Liu, Yu Qiao, Tao Xiang, and Chen Change Loy. Domain generalization: A survey. *IEEE Transactions on Pattern Analysis and Machine Intelligence*, 2022. 2
- [60] Kaiyang Zhou, Yongxin Yang, Timothy Hospedales, and Tao Xiang. Deep domain-adversarial image generation for domain generalisation. In *Proceedings of the AAAI Conference on Artificial Intelligence*, pages 13025–13032, 2020. 5
- [61] Kaiyang Zhou, Yongxin Yang, Yu Qiao, and Tao Xiang. Domain generalization with mixstyle. In *International Conference on Learning Representations*, 2021. 1, 2